

Local Description of the Three-dimensional Wake Transition

Andrey I. Alekseyuk^{a,b,*}, Victor Ya. Shkadov^a

^a*Faculty of Mechanics and Mathematics, Lomonosov Moscow State University, Moscow 119991, Russian Federation*

^b*Water Problems Institute, Russian Academy of Sciences, Moscow 119333, Russian Federation*

Abstract

Mechanisms affecting the transition to three-dimensionality in a cylinder wake are studied based on the local description of the perturbations development for modes A and B. Early stages of three-dimensional vortex structures growth are simulated by the direct numerical solution of the Navier-Stokes equations. The influence of basic mechanisms (such as vorticity diffusion, stretching and tilting of vortex lines) on the growth and decay of perturbations in fluid particles, and on the change in the direction of generated longitudinal vorticity vectors is considered. The same analysis is carried out for an idealized elliptic flow, which reveals qualitative similarities and differences in the perturbations development inside the forming vortex and for the flow with elliptical streamlines. It was shown that the line, along which perturbations of mode B concentrate, can be approximately found based on a two-dimensional solution. The instability of mode B is studied by introducing a simplified two-dimensional flow, which approximates the flow in the braid shear layer. Based on the linear stability analysis of this flow it can be assumed that the curvature of the braid shear layer plays an important role in the mode B instability.

Keywords: secondary instability, wake transition, three-dimensional wake, Navier–Stokes equations

1. Introduction

It is well known that the transition to three-dimensionality in the flow behind a circular cylinder includes two stages of stability loss, called modes A and B [1]. Despite the fact that the publication on the existence of two modes appeared more than 30 years ago, their physical nature is still under discussion: the mechanism triggering the instability when the Reynolds number exceeds the critical one has not been finally established yet.

The critical question on the nature of the first three-dimensional instability (mode A) is what the role of the braid shear layer is. In this region perturbations are growing intensively. It is commonly believed that in this area previously developed perturbations are simply amplified [2, 3]. In its turn they appear in the vortex cores of forming vortices [2, 4, 5]. The studies mentioned above form the basis for the hypothesis that the elliptic instability of the vortex cores is likely to trigger the three-dimensional transition, and that the amplification in the braid regions, resulting in the formation of intense longitudinal vorticity, is the secondary effect.

Nevertheless, other hypotheses of the three-dimensional transition are allowed, since there is still no cogent description of the instability in the localized flow in the vortex formation region: namely, a forming vortex and braid region. One can assume, that the flow instability in the braid shear layer is the trigger of the three-dimensional transition and elliptic instability is the secondary effect. The perturbations generated in the braid shear layer could create special conditions on the boundary of an elliptic flow in the vortex cores, without it such a flow could be stable. Apparently this is the case with the appearance of elliptic instability-like three-dimensional structures in the developed wake. Indeed, in a more recent work [6] it was shown that the flow in a developed wake is linearly stable, when Re is close to a critical value. Hence, in the real flow the appearance of three-dimensional structures in vortex cores of a developed wake can be caused by the previously formed perturbations in the braid shear layer, which create special conditions for the development of the elliptic instability-like structures.

The nature of the second three-dimensional instability (mode B) is associated with the instability of braid regions [2, 4, 5, 7]. However, there are still no theoretical estimations of the local instability of such flows, which predict critical parameters well. The study of mode B is complicated by the fact that it usually develops together with the perturbations of mode A, since the critical Reynolds number for mode A is smaller than for mode B. In numerical simulations it is possible to obtain ‘pure’ mode B excluding linearly unstable perturbations of mode A, by reducing the computational domain in the spanwise direction and using periodic or symmetry conditions on the spanwise boundaries, see, for example, [8, 9].

*Corresponding author.

Email addresses: alekseyuk@mech.math.msu.su (Andrey I. Alekseyuk), shkadov@mech.math.msu.su (Victor Ya. Shkadov)

More detailed reviews on the properties of modes A and B, the physical reasons of three-dimensional transition and routes to turbulence can be found in the papers mentioned above, as well as in many other studies, for example, see [10–15].

The present paper focuses on the description of the early stages of the three-dimensional transition for modes A and B using local characteristics of the two-dimensional base flow. We apply the approach suggested in [9] to analyze the evolution of three-dimensional perturbations of modes A and B in fluid particles based on the action of four mechanisms: the stretching of the vortex lines of perturbations by the base flow; shear deformations of the vortex lines of the base flow by perturbations; viscous diffusion of perturbations; solid-state rotation of fluid particles. Another approach is used to describe the mode B instability by constructing a simplified flow, which approximates the flow in the braid shear layer.

The main part of the paper is divided into four sections. In Sections 2 and 3 we briefly describe the problem formulation, the numerical method and the approach to studying the development of perturbations in a fluid particle. The results for modes A and B are presented separately in Sections 4 and 5. Details on the evolution of perturbations in fluid particles are provided for both modes. For mode A we carry out the comparison of the flow inside a forming vortex and an idealized elliptic flow, which is commonly used to estimate the characteristics of the vortex core instability. We present new ideas on the mechanisms of mode B instability studying rough approximation of the flow in the braid shear layer. The method for linear stability analysis of this simplified flow is described in Appendix A.

2. Numerical simulation

The problem under consideration in this paper is that an infinitely long circular cylinder is placed in the uniform cross flow with velocity U_∞ . The flow regime is defined by the Reynolds number $\text{Re} = U_\infty d/\nu$, where d and ν are the cylinder diameter and the kinematic viscosity. The Cartesian coordinate system (x_1, x_2, x_3) is fixed to a circular cylinder with axis x_3 coinciding with the axis of the cylinder. At infinity the flow is uniform and directed along the x_1 axis. On the cylinder surface velocity vector \mathbf{u} equals zero. At the artificial boundaries in the spanwise direction $x_3 = \pm L/2$ we use symmetry conditions.

The numerical simulations are based on solving Navier-Stokes equations for a viscous perfect gas. The nondimensionalization is based on the diameter of the cylinder d and free-stream velocity U_∞ . For the considered flow regimes compressibility effects are not important, that is why we do not focus on the relevant parameters here (they can be found in [9], the Mach and Prandtl numbers are equal to 0.1 and 0.72). The problem is solved by a stabilized finite-element method on unstructured tetrahedral meshes (and triangular meshes for two-dimensional simulations). More details can be found in [9].

3. Basic mechanisms governing the perturbations development in a fluid particle

We are interested in the early stages of three-dimensionality development in time, when perturbations are relatively small. To describe the development of small perturbations, we use a system of equations in terms of velocity \mathbf{u} and vorticity $\boldsymbol{\omega} = \nabla \times \mathbf{u}$. The base two-dimensional flow can be characterized by the following parameters: vorticity $\boldsymbol{\Omega}(x_1, x_2, t) = \Omega \mathbf{e}_3$; the positive eigenvalue $S(x_1, x_2, t)$ of the strain rate tensor; and the angle $\Phi(x_1, x_2, t)$ between the principal direction and the x_1 axis. Since the perturbations are small and due to symmetry boundary conditions in the spanwise direction, we use the following expressions for velocity and vorticity fields.

$$\begin{aligned} \mathbf{u}(x_1, x_2, x_3, t) &= \mathbf{U}(x_1, x_2, t) + \mathbf{v}(x_1, x_2, t) \sin \gamma x_3 + v_3(x_1, x_2, t) \mathbf{e}_3 \cos \gamma x_3, \\ \boldsymbol{\omega}(x_1, x_2, x_3, t) &= \boldsymbol{\Omega}(x_1, x_2, t) + \boldsymbol{\zeta}(x_1, x_2, t) \cos \gamma x_3 + \zeta_3(x_1, x_2, t) \mathbf{e}_3 \sin \gamma x_3, \end{aligned} \quad (1)$$

here, $\mathbf{U}(x_1, x_2, t) = U_1 \mathbf{e}_1 + U_2 \mathbf{e}_2$ is the velocity of the base flow; additional terms in Eq. (1) describe small perturbations; $\mathbf{v} = v_1 \mathbf{e}_1 + v_2 \mathbf{e}_2 = v(\cos \theta_1 \mathbf{e}_1 + \sin \theta_1 \mathbf{e}_2)$, $\boldsymbol{\zeta} = \zeta_1 \mathbf{e}_1 + \zeta_2 \mathbf{e}_2 = \zeta(\cos \theta \mathbf{e}_1 + \sin \theta \mathbf{e}_2)$ are vectors in $x_1 x_2$ plane; $\gamma = \pi/L$; \mathbf{e}_i are the unit vectors along the x_i -axis, $i = 1, 2, 3$.

The linearization of the vorticity transport equation with respect to the perturbations after some transformations leads to the following equations [9].

$$\frac{D \ln \zeta}{Dt} = \underbrace{S \cos 2\alpha}_{\mathcal{S}_\zeta} + \underbrace{\frac{\gamma \Omega v}{\zeta} \cos \beta}_{\mathcal{V}_\zeta} + \underbrace{\frac{1}{\zeta^2 \text{Re}} (\boldsymbol{\zeta} \cdot \nabla^2 \boldsymbol{\zeta} - \gamma^2 \zeta^2)}_{\mathcal{D}_\zeta}, \quad (2)$$

$$\frac{D\theta}{Dt} = \underbrace{-S \sin 2\alpha}_{\mathcal{S}_\theta} + \underbrace{\frac{\gamma \Omega v}{\zeta} \sin \beta}_{\mathcal{V}_\theta} + \underbrace{\frac{1}{\zeta^2 \text{Re}} (\boldsymbol{\zeta} \times \nabla^2 \boldsymbol{\zeta}) \cdot \mathbf{e}_3}_{\mathcal{D}_\theta} + \underbrace{\frac{1}{2} \Omega}_{\mathcal{R}_\theta}. \quad (3)$$

Here, $D/Dt = \partial/\partial t + \mathbf{u} \cdot \nabla \approx \partial/\partial t + \mathbf{U} \cdot \nabla$ is a linearized substantial derivative. To close the system of equations, the relationship between the vorticity vector and the velocity can be used, $\gamma \boldsymbol{\zeta} = (\nabla \cdot \mathbf{v}_{2,2} - \gamma^2 v_2) \mathbf{e}_1 + (\gamma^2 v_1 - \nabla \cdot \mathbf{v}_{1,1}) \mathbf{e}_2$. Here, to describe the

directions of perturbations vectors \mathbf{v} , $\boldsymbol{\zeta}$ relative to the base flow, we introduce additional angles: angle α between the principal axis and $\boldsymbol{\zeta}$, $\alpha = \theta - \Phi$ and angle β between vectors $\boldsymbol{\zeta}$ and \mathbf{v} , $\beta = \theta_1 - \theta$.

All functions in Eqs. (2) and (3) depend only on x_1 , x_2 , t and base flow parameters are included in the non-differential form. One can also see that the x_3 projections were excluded. The perturbation components along the x_3 axis can be found from the relations $\gamma v_3 = v_{1,1} + v_{2,2}$ and $\gamma \zeta_3 = -\zeta_{1,1} - \zeta_{2,2}$.

The form of Eqs. (2) and (3) for the perturbations allows us to consider quantities ζ and θ in the Lagrangian description as the characteristics associated with a particular fluid particle of the base flow. The rate of amplitude or angle change in a fluid particle can be described with 3 or 4 terms, having a clear connection with the basic physical mechanisms that determine the development of vorticity in the flow: *the first term* (\mathcal{S}_ζ , \mathcal{S}_θ) describes the mechanism of the perturbations vortex lines stretching by the base flow; *the second term* (\mathcal{V}_ζ , \mathcal{V}_θ) is related to spanwise shear deformations of the base flow vortex lines by perturbations; *the third term* (\mathcal{D}_ζ , \mathcal{D}_θ) describes the action of viscous diffusion; *the fourth term* (\mathcal{R}_θ) is the rotation of a fluid particle as a rigid body, which changes only the direction of the vorticity vector $\boldsymbol{\zeta}$.

Having numerical solutions in a three-dimensional formulation, we find all necessary values on the right-hand side using the Fourier series expansion. Then we assess to what extent and in what regions each physical mechanism has a stabilizing or destabilizing effect on the flow. The reasons of the transition are determined by the flow inside the vortex formation region, that is why in Sections 4 and 5 we focus on the processes in the near wake with $x_1 < 3$.

In the discussion of the results it is convenient to distinguish elliptic and hyperbolic subregions of the flow. If $Q = \Omega^2/4 - S^2 > 0$, then rotation prevails; if $Q < 0$, then the stretching rate prevails. The regions with $Q > 0$ and $Q < 0$ are called elliptic and hyperbolic flow regions respectively.

4. Mode A

The development of mode A perturbations can be described as follows, see [9] for details. Perturbations begin to grow in the elliptic region of the forming vortex. Then they grow intensively in the hyperbolic region of the braid shear layer and induce perturbations in a new forming vortex. The process repeats. One can follow the change in the local maximum value of the perturbations amplitude ζ_{\max} as time increases. Two stages of growth with different growth rates are observed.

The first stage of perturbations growth is observed inside the new forming vortex. The first part of this stage corresponds to the appearance of perturbations inside this vortex, and the growth is happening because of the shear deformation of the base flow (\mathcal{V}_ζ , \mathcal{V}_θ). That is why it supports the explanation of self-sustaining process previously suggested by (author?) [4]: perturbations are induced by the deformation of a new vortex by the perturbations existing inside the downstream one. Further at the first stage the situation inside the forming vortex is changing: the growth is connected with the vortex line stretching (\mathcal{S}_ζ , \mathcal{S}_θ).

Then the second stage of growth begins, which is more intense than the first one. This stage starts when perturbations are leaving the core of the forming vortex. The reason of growth is the first mechanism, that is vortex line stretching (\mathcal{S}_ζ , \mathcal{S}_θ). Once the forming vortex is shed perturbations in braids regions are fading out.

The described process can be seen in Fig. 1, which shows vectors $\boldsymbol{\zeta}$, \mathbf{v} and the principal direction of the strain rate tensor at different points in the near wake. From Eq. (2) it follows, that the more aligned the principal direction and the direction of $\boldsymbol{\zeta}$, the greater the growth of perturbations due to the stretching mechanism \mathcal{S}_ζ and from (3) one can see that term \mathcal{S}_θ tends to reduce the angle between them. The more the angle between vectors \mathbf{v} and $\boldsymbol{\zeta}$ differs from the right angle, the more pronounced the action of shear deformations \mathcal{V}_ζ is. Whether this will be growth or decay depends on the sign of $\Omega \cos \beta$, just as the sign of $\Omega \sin \beta$ determines in which direction this mechanism (\mathcal{V}_θ) tends to rotate vector $\boldsymbol{\zeta}$. For example, the interaction of perturbations fields between downstream and upstream vortices is clearly observed in Fig. 1 a, b. At the vicinity of the boundary between two vortices $\cos \beta$ significantly differs from 0. That is why the action of the shear deformation mechanism is pronounced. Likewise, the action of this mechanism is pronounced in the braid shear layer (Fig. 1 c, d), however, it has mostly a stabilizing effect.

Another observation is that for mode A the flow in the braid shear layer is organized so that the principal direction and vector $\boldsymbol{\zeta}$ are not aligned. The non-alignment together with the more pronounced action of the shear deformation mechanism (\mathcal{V}_θ) determine the main differences between the development of perturbations in the braid shear layer for modes A and B (in Fig. 3 we will see that the principal direction and vector $\boldsymbol{\zeta}$ are mostly aligned and $\cos \beta$ is closer to zero for mode B).

Such information on the local description of perturbations can be useful in constructing or validating the simplified models of the flow instability. Next we apply this approach to describe the theoretical solution for an idealized elliptic instability, which can be used to build estimates of vortex core instability [4, 5, 16, 17]. The base flow is described by velocity field

$$\mathbf{U} = -\left(\frac{1}{2}\Omega + S\right)x_2\mathbf{e}_1 + \left(\frac{1}{2}\Omega - S\right)x_1\mathbf{e}_2, \quad (4)$$

which is the exact solution of Navier-Stokes equations [18], here, Ω and S are constant. In the case of vanishing strain it

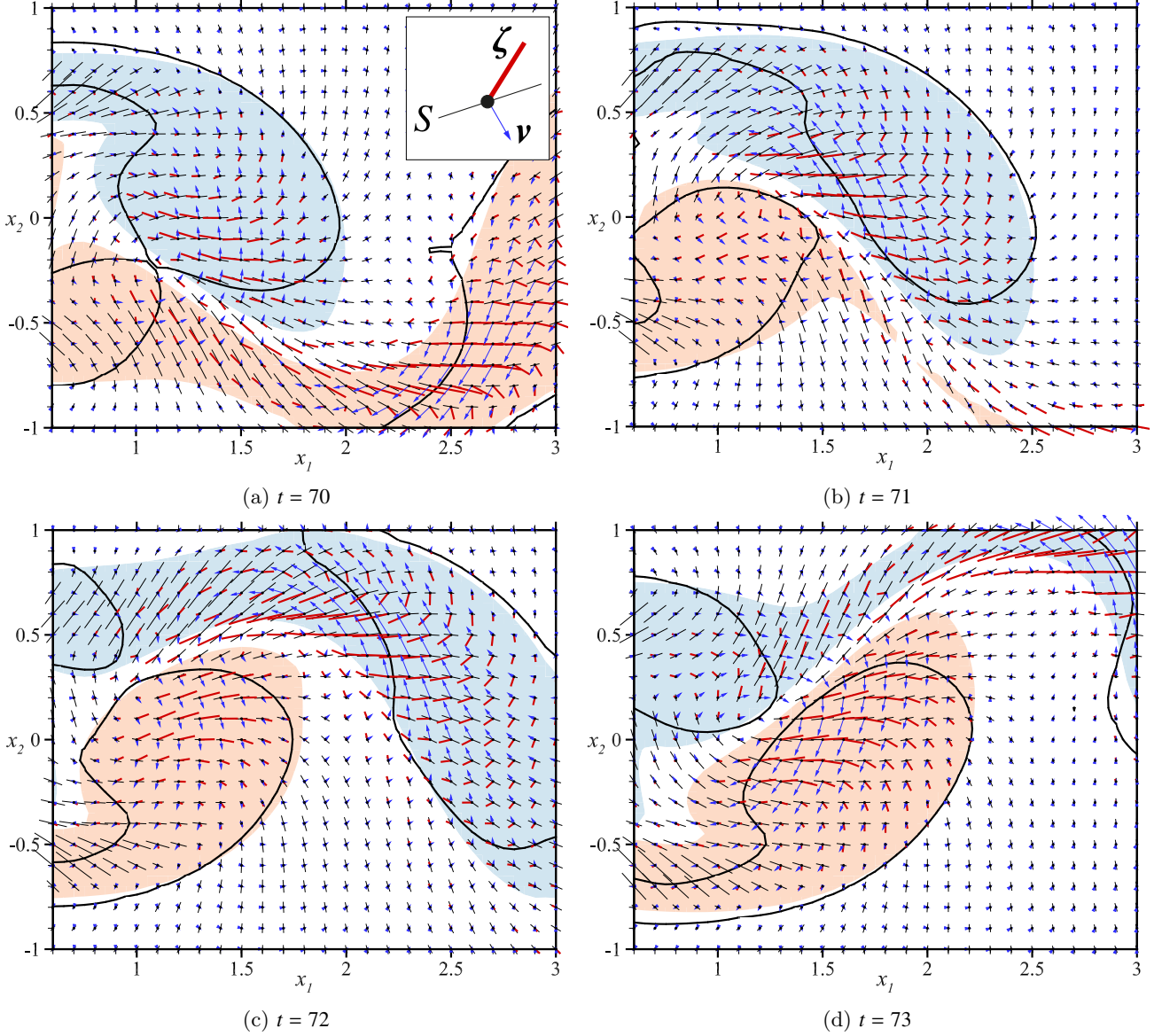


Fig. 1: Perturbations evolution for Mode A at $\text{Re} = 220$ and $L = 2$. Filled regions are the regions of $|\Omega| \geq 1$; solid lines correspond to isolines $Q = 0$; blue arrows and thick red solid lines are vectors \mathbf{v} and $\boldsymbol{\zeta}$, their tails are placed in the dots, which correspond to the considered fluid particles; thin solid lines indicate the principal direction, their length is proportional to the value of S . The following proportion is used for the lengths of the segments $|\mathbf{v}| : |\boldsymbol{\zeta}| = 1 : 2$. (For interpretation of the references to color in this figure legend, the reader is referred to the web version of this article.)

is possible to obtain an approximate solution for perturbations [19],

$$\begin{aligned} \mathbf{v} &= -C \frac{\sqrt{3}}{2} e^{\sigma t} \left[\left(J_0 + \frac{J_2}{3} \right) \sin \left(\varphi + \frac{\pi}{4} \right) \mathbf{e}_r + \left(J_0 - \frac{J_2}{3} \right) \cos \left(\varphi + \frac{\pi}{4} \right) \mathbf{e}_\varphi \right] \\ \boldsymbol{\zeta} &= C \sqrt{3} \gamma e^{\sigma t} \left[\left(J_0 + \frac{J_2}{3} \right) \cos \left(\varphi + \frac{\pi}{4} \right) \mathbf{e}_r - \left(J_0 - \frac{J_2}{3} \right) \sin \left(\varphi + \frac{\pi}{4} \right) \mathbf{e}_\varphi \right] \end{aligned} \quad (5)$$

Here, J_0 and J_2 are the first kind Bessel functions of argument $\sqrt{3}\gamma r$; r, φ are polar coordinates; $\mathbf{e}_r, \mathbf{e}_\varphi$ are unit vectors along polar coordinates r and φ ; σ is the growth rate, the theoretical expression for which can be found in [16, 19]; C is a constant; sign ‘-’ is used in the first equation because we shifted the solution from [19] along the x_3 axis by $\pi/(2\gamma)$.

Figure 2 shows the action of the basic mechanisms ($\mathcal{S}_\zeta, \mathcal{V}_\zeta$) and perturbations vectors for an idealized elliptic flow and for the flow inside the upstream forming vortex in Fig. 1c (the coordinate system for the forming vortex is rotated so that the principal direction angle approximately equals 45 degrees as for an idealized flow). The parameters of the idealized flow Ω, S, γ in Eqs. (4), (5) correspond to the considered case from direct numerical simulations.

The qualitative comparison in Fig. 2 shows, that these solutions turned out to be clearly different. One can see two (Fig. 2c) and four (Fig. 2f) regions of growth and decay caused by shear deformations (\mathcal{V}_ζ). However, as for an idealized

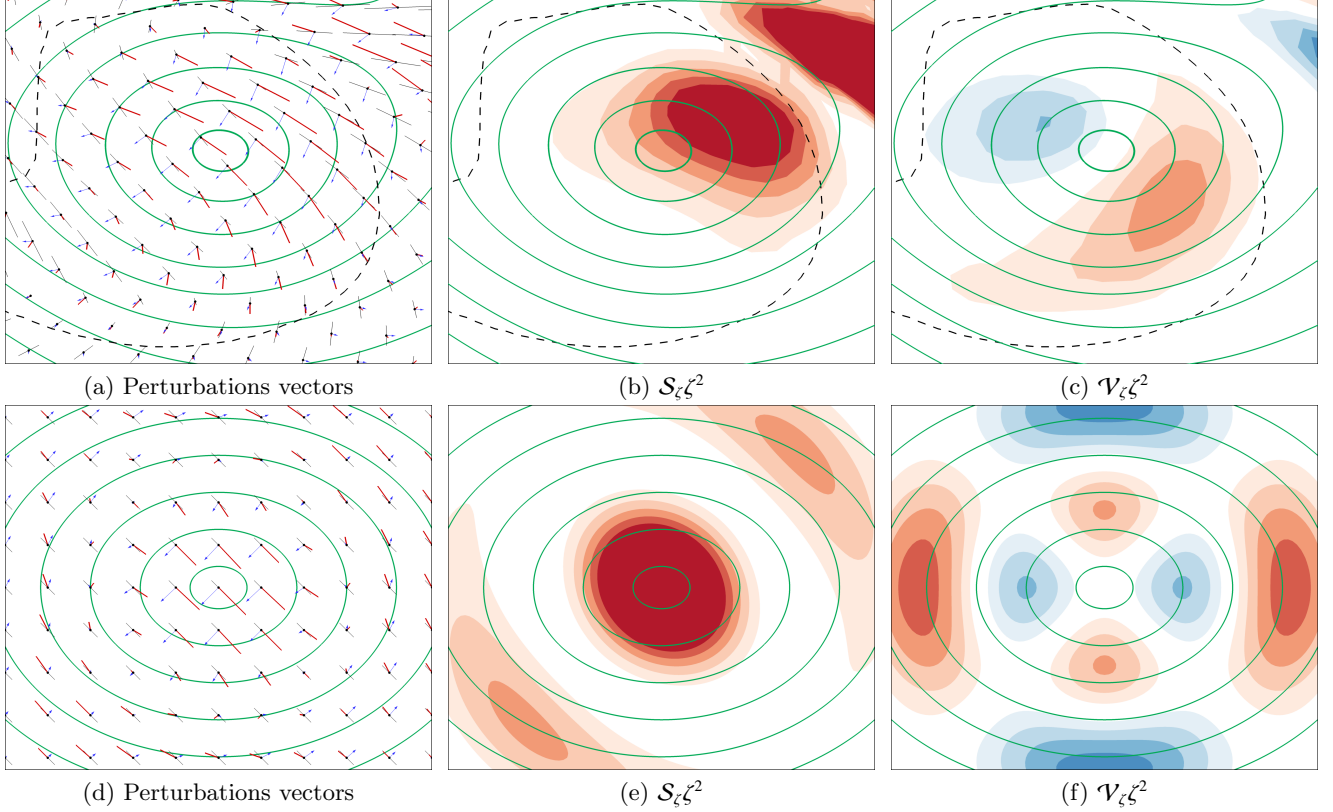


Fig. 2: The comparison of perturbations development inside the forming vortex at $\text{Re} = 220$, $L = 2$, $t = 72$ (a-c) and for an idealized elliptic instability (d-f). Blue arrows and thick red solid lines are vectors \mathbf{v} and $\boldsymbol{\zeta}$, their tails are placed in the dots, which correspond to the considered fluid particles; thin solid lines indicate the principal direction. The following proportion is used for the lengths of the segments in plots (a) and (b), $|\mathbf{v}| : |\boldsymbol{\zeta}| = 1 : 2$. Red and blue colors in plots (b), (c), (e), (f) correspond to the positive and negative action of basic mechanisms \mathcal{S}_ζ , \mathcal{V}_ζ . Solid green lines are streamlines, the dashed line in plots (a)-(c) is isoline $Q = 0$. (For interpretation of the references to color in this figure legend, the reader is referred to the web version of this article.)

flow it seems that the action of this mechanism in Fig. 2c is almost canceled out while a fluid particle passes along the elliptic contour. And the growth is related to the stretching of vortex lines (\mathcal{S}_ζ). The difference in distribution of \mathcal{V}_ζ as well as the shift of the perturbed region relative to the vortex center can be caused by disturbed conditions on the boundary of the elliptic region and by the fact that this region is finite, opposite to the considered idealized flow. It may be possible to resolve these discrepancies by constructing the localized solution, see [19, 20].

5. Mode B

For mode B the process of perturbations development takes place mostly outside the elliptic regions and there is only one stage of growth [9]. The growth is caused by the vortex line stretching mechanism (\mathcal{S}_ζ). Perturbations in braid regions are fading out when a vortex is shed in the wake.

The development of perturbations vectors \mathbf{v} and $\boldsymbol{\zeta}$ is shown in Fig. 3. Since the angle between vectors \mathbf{v} and $\boldsymbol{\zeta}$ is close to the right one the contribution of the shear deformation mechanism (\mathcal{V}_ζ) to perturbations growth/decay is insignificant in comparison to the contribution of the stretching mechanism. Unlike mode A, the direction of vorticity vector rotation is mostly defined by the shear deformation of the base flow and rigid body rotation, because the directions of the principal axis and vorticity vector almost coincide. Therefore, the rotation of the principal direction in a fluid particle and the rotation of $\boldsymbol{\zeta}$ because of the shear deformation (\mathcal{V}_θ) and rigid body rotation (\mathcal{R}_θ) mechanisms are almost synchronized.

We are going to give a rough description of mode B instability by analyzing a simplified flow approximating the local flow, where perturbations of mode B appear. One can notice that perturbations are elongated along some line (further ‘core line’), which can be defined as the line with the spanwise velocity equal to zero, $u_3 = 0$, see Fig. 4a. Thus we assume that for the instability of the braid shear layer the dependence of the base flow on the coordinate across the core line is more significant than along it. When a simplified flow is reconstructed from the two-dimensional one there is no information on the core line. However, it was found out that the core line is close to the line where the action of diffusion is zero $\nabla^2 \Omega = 0$, Fig. 4a. This makes it possible to approximately identify this line based on a two-dimensional flow. Further we use line $\nabla^2 \Omega = 0$ as a definition for the core line. Figure 5 shows this line and the isolines $\Omega = \pm 0.5$ at various Re . As Re increases the length of vortex formation region decreases (Fig. 5a) and as a result the curvature of the core line increases (Fig. 5b).

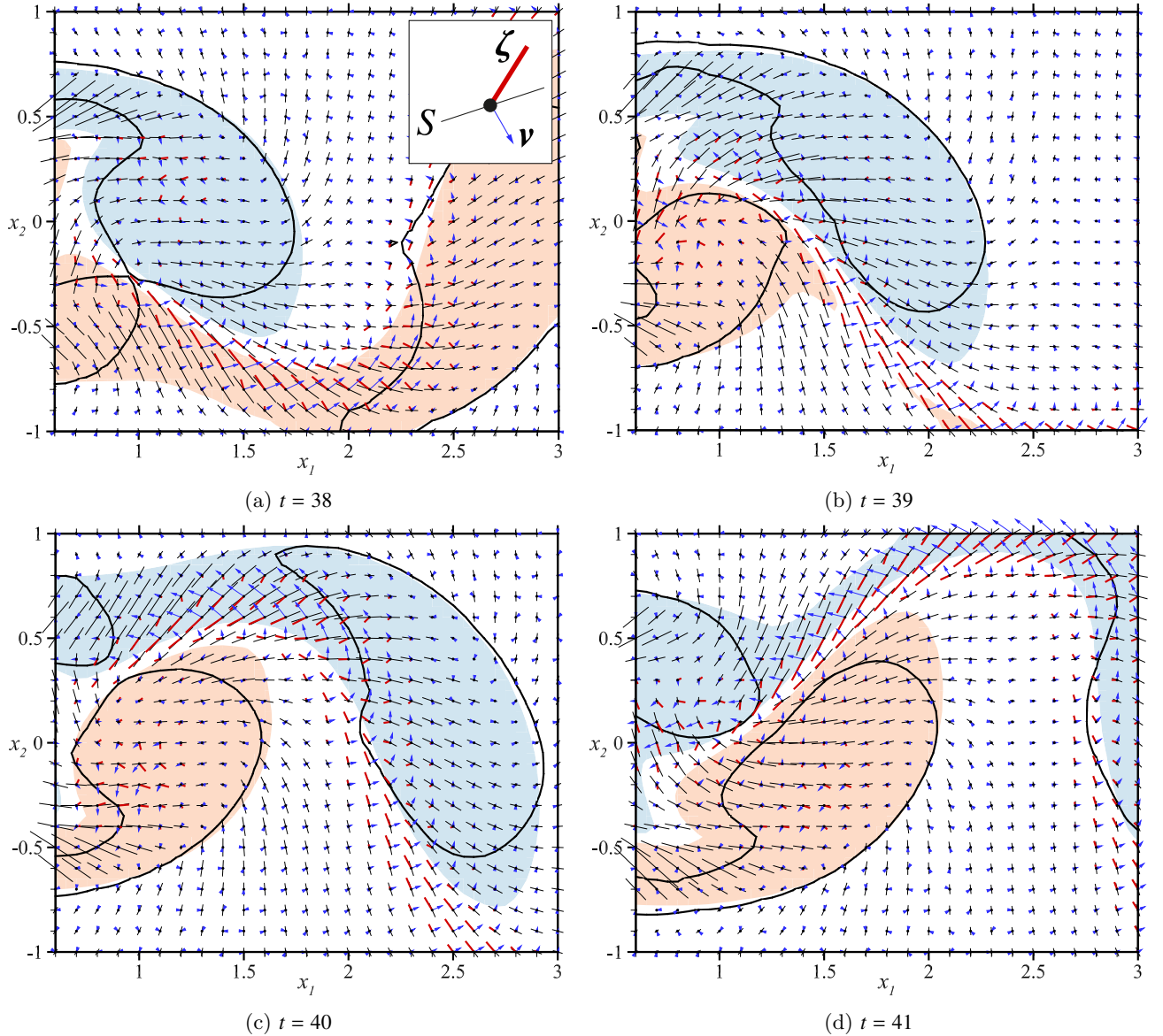


Fig. 3: Perturbations evolution for Mode B at $\text{Re} = 300$ and $L = 0.4$. Filled regions are the regions of $|\Omega| \geq 1$; solid lines correspond to isolines $Q = 0$; blue arrows and thick red solid lines are vectors \mathbf{v} and $\boldsymbol{\zeta}$, their tails are placed in the dots, which correspond to the considered fluid particles; thin solid lines indicate the principal direction, their length is proportional to the value of S . The following proportion is used for the lengths of the segments $|\mathbf{v}| : |\boldsymbol{\zeta}| = 1 : 10$. (For interpretation of the references to color in this figure legend, the reader is referred to the web version of this article.)

Let us consider the simplified one-dimensional base flow in polar coordinates (r, φ) , Fig. 4b. The flow is defined in the annular layer $R - \delta \leq r \leq R + \delta$, here R is a curvature radius of the core line in the point under consideration; δ is constant. We assume that the flow is stationary and it depends only on radial coordinate r . The latter assumption can be supported by an observation on the weak dependence of mutual arrangement of vectors $\boldsymbol{\zeta}$, \mathbf{v} and the principal direction on the coordinate along core line in the region, where perturbations grow intensively (Fig. 3). The normal $u_r = V(r)$ and tangential $u_\varphi = U(r)$ velocity components across the layer are equal to the ones across the core line (in the real flow) in a moving coordinate system, at which the core line is locally fixed. The choice of such a coordinate system was made qualitatively (since the core line is deforming in time), hence, uncertainty is introduced. Figure 6 shows the normal and tangential velocity profiles for various points on the core line (Fig. 5b) at $\text{Re} = 100, 200, 300$ and time t corresponding to the intensive growth of perturbations in the braid region. The qualitative behavior of $U(r)$ and $V(r)$ is similar.

The linear stability of the flow is studied by the numerical solution of eigenvalue problem, see Appendix A. The following kind of velocity perturbations are considered: in cylindrical coordinates (r, φ, z)

$$u'_r = e^{\beta t} v_n(r) \sin \gamma z, \quad u'_\varphi = e^{\beta t} v_s(r) \sin \gamma z, \quad u'_z = e^{\beta t} v_z(r) \cos \gamma z.$$

Before discussing the results, it is necessary to make a few comments about the roughness of the approximation. It

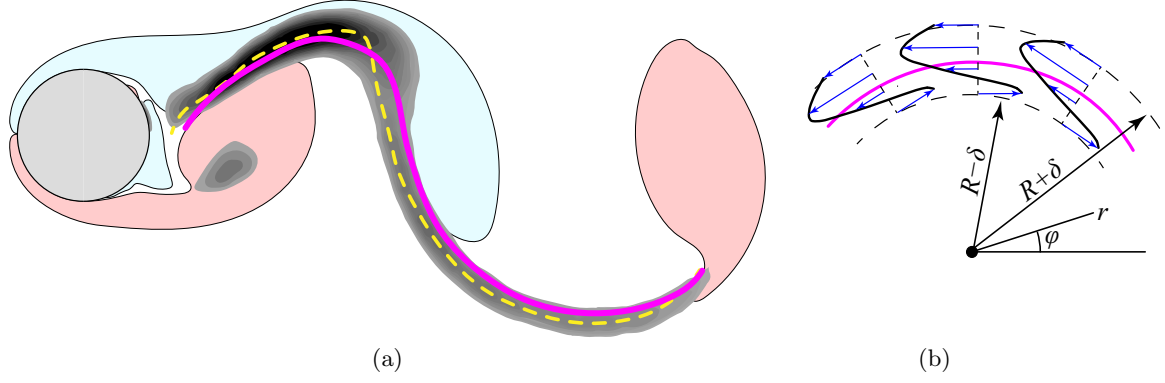


Fig. 4: Reconstruction of the approximation for the braid shear layer flow. On the plot (a) solid (pink) and dashed (yellow) lines are core lines, defined by relations $\nabla^2\Omega = 0$ and $u_3 = 0$; amplitude ζ of vorticity in the streamwise plane is shown with gray regions; vortices of the base flow are pale red and blue regions. Scheme (b) shows a simplified flow in polar coordinates. (For interpretation of the references to color in this figure legend, the reader is referred to the web version of this article.)

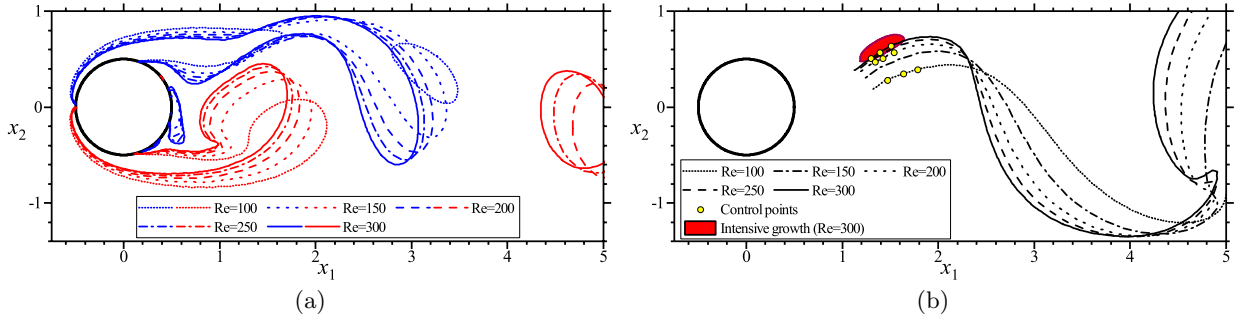


Fig. 5: Vorticity ($\Omega = \pm 0.5$) and core lines (parts of lines $\nabla^2\Omega = 0$) at various Reynolds numbers, $Re = 100, 150, 200, 250, 300$. Value of t for each Re corresponds to zero lift coefficient C_L and $C_{L,t} > 0$. On the plot (b) the circles indicate the control points, which are used to construct a simplified flow (the points are numbered from left to right); the subregion of the most intensive growth of perturbations at $Re = 300$ is filled in red. (For interpretation of the references to color in this figure legend, the reader is referred to the web version of this article.)

does not accurately describe the real flow, since the flow is changing along the core line, it is not stationary and the core line is moving and deforming in time. The simplified base flow by itself is not a solution of the Navier-Stokes equations, however it could be an approximation of it. The curvature of the core line and the coordinate system fitted to this line are obtained qualitatively. Nevertheless, the stability analysis gives the results consistent with the real data on mode B instability and that is why the simplified flow might contain some of the necessary physics.

The results of linear stability analysis are shown in Fig. 7. At $Re = 300$ and fixed radius of curvature, $R = 1$, the predicted wavenumber γ_* (with maximum value of β) varies between 5.2 and 6 (Fig. 7a), which corresponds to wavelengths $1.05 \leq \lambda_* \leq 1.21$. The change of the sections does not significantly change γ_* , however, it changes β and the range of unstable wavenumbers γ .

The increase in δ leads to the reduction in γ_* (Fig. 7 a). It is not clear what the right choice for δ is, since if it is too big the velocity profiles begin to contain flow properties not related to the braid shear layer. One might have to choose the value close to 0.4, which corresponds to a characteristic length scale for vortex structures of mode B. The value $\delta = 0.4$ and $R = 1$ leads to $\lambda_* \approx 1$, which is close to the theoretical value. However, the increase of R leads to smaller values of γ_* , and, hence, to a worse agreement (Fig. 7 b). The idealized flow becomes more stable as Re decreases or the radius of curvature increases (Fig. 7 b, c). In particular, the flow is stable if $Re = 100$.

These results show a scatter of critical parameters, which makes it difficult to obtain quantitative estimates. However, with a certain choice of model parameters the results are in qualitative agreement with the real data. And more importantly, the analysis gives one an idea on the influence of the Re and R on such flows. Having this one can assume that the instability of the braid shear layer is related to its curvature which becomes greater as Re increases (Fig. 5b), due to the reduction of the length of the vortex formation region (Fig. 5a). With the increase of the curvature the braid shear layer becomes more unstable (Fig. 7b). In its turn the velocity profiles themselves become more unstable as Re increases (Fig. 7c), however, in the limit $R \rightarrow \infty$ they are stable (Fig. 7b). That is why the instability of mode B could be caused by the instability of the braid shear layers that are curved enough.

In [7] the centrifugal instability was discussed as a possible reason for the emergence of Mode B instability. The results of this section can be interpreted as some support of their reasoning, since the action of the centrifugal forces should be more pronounced with the increasing velocity and decreasing curvature radius. Both happen with the increase in the

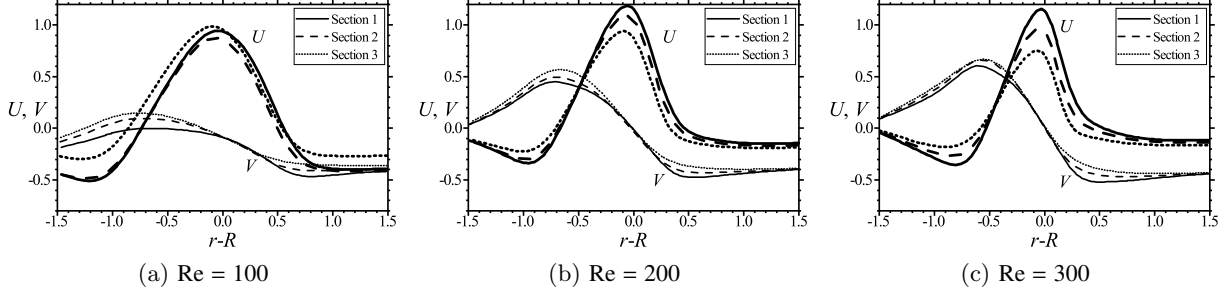


Fig. 6: Velocity profiles for an idealized base flow for various sections of the braid shear layer (shown with circles in Fig. 5 b) at $Re = 100, 200, 300$.

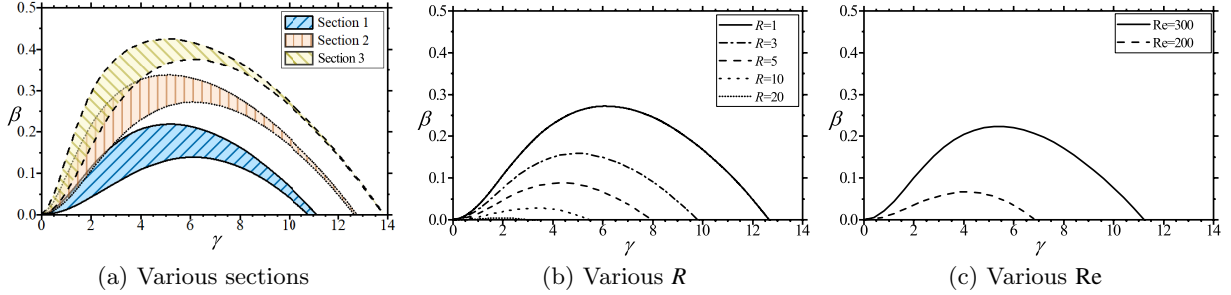


Fig. 7: Linear stability analysis of an idealized flow for various (a) sections of the braid shear layer at $Re = 300, R = 1$, the filled area shows the scatter of the curve $\beta(\gamma)$ as δ changes in the range $[0.4, 0.8]$; (b) radii of curvature at $Re = 300, \delta = 0.4$, 2nd section; (c) Reynolds numbers at $R = 2, \delta = 0.4$, 2nd section (flow is stable if $Re = 100$).

Reynolds number, as can be seen in Figs. 5b and 6.

6. Conclusions

The three-dimensional transition in the near wake behind a circular cylinder is described based on the local characteristics of the flow. The previous results on the analysis of basic mechanisms affecting the growth and decay of perturbations in a fluid particle for modes A and B [9] were supplemented by the consideration of the mutual arrangement of perturbations vectors \mathbf{v} , $\boldsymbol{\zeta}$ and base flow parameters S and $\boldsymbol{\Omega}$. Thus, the reasons of change in the direction of longitudinal vorticity vector $\boldsymbol{\zeta}$ can be traced. In particular, it was shown that, for the braid shear layer instability (mode B) the perturbations $\boldsymbol{\zeta}$ are mostly aligned with the principal direction of the strain rate tensor. The distribution of the principal direction is significantly non-uniform in the hyperbolic region. That is why the rotation of the principal direction in fluid particles is synchronized with the rotation of $\boldsymbol{\zeta}$ due to the action of the shear deformation (\mathcal{V}_θ) and rigid body rotation (\mathcal{R}_θ) mechanisms. For mode A the process of the perturbations growth in the braid shear layer is different: $\boldsymbol{\zeta}$ and the principal direction is not aligned, and the angle between $\boldsymbol{\zeta}$ and \mathbf{v} is significantly different from the right angle, which is manifested in the spanwise waviness of the hyperbolic region caused by shear deformations (\mathcal{V}_θ).

This approach was also applied to an idealized flow with elliptic streamlines, due to the fact that three-dimensional instability of such a flow is usually associated with the instability of mode A. The qualitative difference was observed in the action of the shear deformation mechanism (\mathcal{V}_θ) for the idealized flow (in the case of vanishing strain) and the flow inside the forming vortex. Perhaps, this issue can be overcome by constructing the solution in the finite elliptic domain with certain conditions on its boundary.

It was found that the core line along which perturbations of mode B concentrate could be well approximated by the line of zero vorticity diffusion, $\nabla^2 \boldsymbol{\Omega} = 0$. This allows to choose a region where three-dimensional perturbations may develop based only on the parameters of the two-dimensional flow. The instability of braid shear layers was studied assuming that the dependence of the base flow across the core line is more significant than along it. A rough approximation of the region with the most intensive growth by a stationary one-dimensional flow was proposed. The linear stability analysis of such idealized flows gives a general idea of the flow dependence in the hyperbolic region on the Reynolds number and the radius of curvature. It allowed us to assume that the instability of mode B is related to the curvature of the braid shear layers.

Acknowledgements

The research is carried out using the equipment of the shared research facilities of HPC computing resources at Lomonosov Moscow State University. This work was supported by the grants of the Russian Foundation for Basic Research

Appendix A. Linear stability analysis of an idealized flow for mode B

For a solution, which does not depend on φ , the Navier-Stokes equations in polar coordinates (r, φ, z) can be written as

$$\begin{cases} u_{r,t} + u_r u_{r,r} + u_z u_{r,z} - \frac{1}{r} u_\varphi^2 = -p_{,r} + \frac{1}{\text{Re}} \left[\frac{1}{r} (ru_{r,r})_{,r} + u_{r,zz} - \frac{1}{r^2} u_r \right], \\ u_{\varphi,t} + u_r u_{\varphi,r} + u_z u_{\varphi,z} + \frac{1}{r} u_r u_\varphi = -\frac{1}{r} p_{,\varphi} + \frac{1}{\text{Re}} \left[\frac{1}{r} (ru_{\varphi,r})_{,r} + u_{\varphi,zz} - \frac{1}{r^2} u_\varphi \right], \\ u_{z,t} + u_r u_{z,r} + u_z u_{z,z} = -p_{,z} + \frac{1}{\text{Re}} \left[\frac{1}{r} (ru_{z,r})_{,r} + u_{z,zz} \right], \\ (ru_r)_{,r} + ru_{z,z} = 0. \end{cases}$$

The perturbed flow is expressed as follows $u_r = V(r) + e^{\beta t} v_n(r) \sin \gamma z$, $u_\varphi = U(r) + e^{\beta t} v_s(r) \sin \gamma z$, $u_z = e^{\beta t} v_z(r) \cos \gamma z$, $p = P(r) + e^{\beta t} q(r) \sin \gamma z$, where the base two-dimensional flow is $u_r = V(r)$, $u_\varphi = U(r)$, $u_z = 0$, $p = P(r)$. Substituting these in the Navier-Stokes equations leads to the following system.

$$\begin{cases} \beta v_n + (Vv_n)' - \frac{2}{r} Uv_s = -q' + \frac{1}{\text{Re}} Lv_n, \\ \beta v_s + \frac{1}{r} V(rv_s)' + \frac{1}{r} (rU)' v_n = \frac{1}{\text{Re}} Lv_s, \\ \beta v_z + Vv_z' = -\gamma q + \frac{1}{\text{Re}} (Lv_z + \frac{1}{r^2} v_z), \\ (rv_n)' - \gamma rv_z = 0. \end{cases}$$

Here, $L(\cdot) = (\cdot)'' + r^{-1}(\cdot)' - r^{-2}(\cdot) - \gamma^2(\cdot)$. Excluding pressure q and velocity component v_z from the system we obtain

$$\begin{cases} \beta w + \frac{2}{r} \gamma^2 Uv_s + [Vw]' - \frac{1}{\text{Re}} Lw = 0, \\ \beta v_s + \frac{1}{r} V(rv_s)' + \frac{1}{r} (rU)' v_n - \frac{1}{\text{Re}} Lv_s = 0, \\ w - Lv_n = 0. \end{cases} \quad (\text{A.1})$$

The spectral problem given by Eqs. (A.1) with eigenvalue β is solved on an annulus $r_1 \leq r \leq r_2$. We assume that at $r = r_1$ and $r = r_2$ perturbations are absent. This problem is solved numerically by the local method (with shooting procedure), for example, described in [21].

References

- [1] C. H. K. Williamson, The existence of two stages in the transition to three-dimensionality of a cylinder wake, *Physics of Fluids* 31 (11) (1988) 3165–3168. doi:10.1063/1.866925.
- [2] M. C. Thompson, T. Leweke, C. H. K. Williamson, The physical mechanism of transition in bluff body wakes, *Journal of Fluids and Structures* 15 (3-4) (2001) 607–616. doi:10.1006/jffs.2000.0369.
- [3] S. Julien, S. Ortiz, J.-M. Chomaz, Secondary instability mechanisms in the wake of a flat plate, *European Journal of Mechanics - B/Fluids* 23 (1) (2004) 157–165. doi:10.1016/j.euromechflu.2003.07.001.
- [4] C. H. K. Williamson, Three-dimensional wake transition, *Journal of Fluid Mechanics* 328 (1996) 345–407. doi:10.1017/S0022112096008750.
- [5] T. Leweke, C. H. K. Williamson, Three-dimensional instabilities in wake transition, *European Journal of Mechanics - B/Fluids* 17 (4) (1998) 571–586. doi:10.1016/S0997-7546(98)80012-5.
- [6] D. Barkley, Confined three-dimensional stability analysis of the cylinder wake, *Physical Review E* 71 (1) (2005) 017301. doi:10.1103/PhysRevE.71.017301.
- [7] K. Ryan, M. C. Thompson, K. Hourigan, Three-dimensional transition in the wake of bluff elongated cylinders, *Journal of Fluid Mechanics* 538 (2005) 1–29. doi:10.1017/S0022112005005082.
- [8] R. D. Henderson, Nonlinear dynamics and pattern formation in turbulent wake transition, *Journal of Fluid Mechanics* 352 (1997) 65–112. doi:10.1017/S0022112097007465.
- [9] A. I. Alekseyuk, V. Y. Shkadov, Analysis of three-dimensional transition mechanisms in the near wake behind a circular cylinder, *European Journal of Mechanics - B/Fluids* 72 (2018) 456–466. doi:10.1016/j.euromechflu.2018.07.011.

- [10] D. Barkley, R. D. Henderson, Three-dimensional Floquet stability analysis of the wake of a circular cylinder, *Journal of Fluid Mechanics* 322 (1996) 215–241. doi:10.1017/S0022112096002777.
- [11] B. R. Noack, H. Eckelmann, A global stability analysis of the steady and periodic cylinder wake, *Journal of Fluid Mechanics* 270 (1994) 297–330. doi:10.1017/S0022112094004283.
- [12] G. E. Karniadakis, G. S. Triantafyllou, Three-dimensional dynamics and transition to turbulence in the wake of bluff objects, *Journal of Fluid Mechanics* 238 (1992) 1–30. doi:10.1017/S0022112092001617.
- [13] H. Persillon, M. Braza, Physical analysis of the transition to turbulence in the wake of a circular cylinder by three-dimensional Navier–Stokes simulation, *Journal of Fluid Mechanics* 365 (1998) 23–88. doi:10.1017/S0022112098001116.
- [14] R. Mittal, S. Balachandar, Generation of Streamwise Vortical Structures in Bluff Body Wakes, *Physical Review Letters* 75 (7) (1995) 1300–1303. doi:10.1103/PhysRevLett.75.1300.
- [15] F. Giannetti, S. Camarri, P. Luchini, Structural sensitivity of the secondary instability in the wake of a circular cylinder, *Journal of Fluid Mechanics* 651 (2010) 319–337. doi:10.1017/S0022112009993946.
- [16] M. J. Landman, P. G. Saffman, The three-dimensional instability of strained vortices in a viscous fluid, *Physics of Fluids* 30 (8) (1987) 2339–2342. doi:10.1063/1.866124.
- [17] T. Leweke, C. H. K. Williamson, Cooperative elliptic instability of a vortex pair, *Journal of Fluid Mechanics* 360 (1998) 85–119. doi:10.1017/S0022112097008331.
- [18] A. D. D. Craik, W. O. Criminale, Evolution of wavelike disturbances in shear flows: A class of exact solutions of the Navier-Stokes equations, *Proceedings of the Royal Society A: Mathematical, Physical and Engineering Sciences* 406 (1830) (1986) 13–26. doi:10.1098/rspa.1986.0061.
- [19] F. Waleffe, On the three-dimensional instability of strained vortices, *Physics of Fluids A: Fluid Dynamics* 2 (1) (1990) 76–80. doi:10.1063/1.857682.
- [20] C. Eloy, S. Le Dizès, Stability of the Rankine vortex in a multipolar strain field, *Physics of Fluids* 13 (3) (2001) 660–676. doi:10.1063/1.1345716.
- [21] P. J. Schmid, D. S. Henningson, *Stability and Transition in Shear Flows*. Volume 142 in Applied Mathematical Sciences, Springer-Verlag, 2001.